Int. J. Multiphase Flow Vol. 16, No. 3, pp. 429–445, 1990
Printed in Great Britain

0301-9322/90 $3.00 + 0.00
Pergamon Press/Elsevier

PHASE SEPARATION OF DISPERSED MIST AND DISPERSED ANNULAR (RIVULET OR THIN FILM) FLOW IN A TEE—I

EXPERIMENTS

G. E. McCREERY
Idaho National Engineering Laboratory, EG&G Idaho Inc., Idaho Falls, ID 83415, U.S.A.

S. BANERJEE
Department of Chemical and Nuclear Engineering, University of California, Santa Barbara, CA 93106, U.S.A.

(*Received* 23 *February* 1989; *in revised from* 25 *November* 1989)

Abstract—An experimental and analytical investigation of dispersed and dispersed annular (rivulet or thin film) flow phase separation in a tee was performed. The primary objective of the experimental portion of the reseach was to obtain data and observations to help formulate and test mechanistically based analytical models of phase separation for these two flow regimes. A variety of measurements were obtained, including: gas velocity profiles; pressure; macroscopic mass balances; streamline and eddy boundary maps; and rivulet, drop and solid particle trajectories.

Key Words: phase separation, tee, dispersed mist flow, dispersed annular flow

INTRODUCTION

Partial or complete phase separation of gas and liquid phases occurs when a two-phase fluid enters a tee and divides into downstream and side-branch pipes or ducts. The phases separate because of differing phasic momentum and body and surface forces. Phase separation is a complicated function of flow rates, qualities, pipe or duct size and orientation etc. In addition, as our research indicates, the primary variables that determine phase separation are flow regime specific.

Phase separation in a tee is of importance to several possible nuclear reactor LOCA scenarios, such as a break in a pipe that tees off the primary coolant loop of PWR. Phase separation is also of importance in the oil, gas and chemical processing industries. The research presented in this article, which deals with experiments, and in part II (McCreery & Banerjee submitted), which deals with analysis, is motivated by, but more general than, the necessity of specifying flow distributions to vacuum buildings in some CANDU (Midvidy 1983) nuclear reactors. A vacuum building is teed off the main passageway in the containment envelope in which fluid would travel following a LOCA. The main passageway and that leading to the vacuum building have rectangular cross-section geometry and are oriented in the horizontal plane. The predominant flow regime expected in the passageways is dispersed mist. At lower gas velocities water drops will de-entrain, liquid will be swept along the walls into the tee and the flow regime will be dispersed annular.

The primary objective of the experimental portion of the research was to obtain experimental data and observations to help formulate and test mechanistic analytical models of phase separation in a tee for dispersed mist and dispersed annular flow. The models calculate liquid drop and liquid pathline trajectories as a means for obtaining macroscopic phase separation quantitites. The application of the experimental results to modeling is frequently mentioned in this article. As a first step, the research on dispersed annular flow was confined to that with liquid rivulets or thin films, where the complications due to liquid momentum are minimized. The experiments concentrated on determining, in order of presentation in this article:

(a) Pressure loss coefficients for given air volumetric flow ratios, Q_3/Q_1, where Q is volumetric flow rate, 3 is side branch and 1 is upstream.
(b) Macroscopic mass balances for dispersed mist air–water flow.
(c) Drop diameter distribution for dispersed mist air–water flow.
(d) Air streamlines and eddy boundaries.
(e) Water rivulet pathlines.
(f) Water drop and solid particle trajectories for drops and particles of known size and velocity.

This article is taken from a larger work (McCreery 1988), which describes the experiments and modeling in detail. The portion of the experiments that offer new and unique results and those results that are necessary to explain the analytical modeling are presented.

The literature survey presented in the larger work indicates that a fairly extensive data base for phase separation in tees exists [another recent summary is given in Seeger *et al.* (1985)]. However, the majority of published phase separation research was found to be inapplicable to our modeling purposes. This was due to: (a) the geometry investigated was, with two exceptions, of circular cross section; (b) the flow regimes examined did not include dispersed mist flow; and (c) only the more macroscopic quantities such as flow rates, qualities and pressure losses were measured. One exception to qualifications (a) and (b) is Popp & Sallet (1983), who investigated bubbly flow in a rectangular geometry, measured velocity profiles, turbulent fluctuations and corner eddy contraction coefficients. The other exception is Lemmonier & Hervieu (1988), who experimentally investigated and analytically modeled bubbly flow in a square cross-section tee. New experiments were needed to investigate not only the macroscopic quantities of flow rates, qualities and pressure losses, but also gas streamlines, liquid pathlines, eddy boundary geometry and for dispersed mist flow, drop size spectra and trajectories of drops (and, alternately, trajectories of solid particles) of known size and velocity.

EXPERIMENTAL APPARATUS AND TECHNIQUES

The experiments were performed in an air–water apparatus consisting of two large air blowers (0.56 m impeller diameters) connected in series to a long rectangular cross-section duct leading to a tee in the horizontal plane. The tee test section is shown in figure 1. The inside dimensions of the duct were 2.5×7.5 cm, with the larger dimension oriented in the horizontal plane. The duct upstream of the tee was 5 m long, which provides a length/hydraulic diameter ratio of 120. This length was sufficient to ensure that fully developed air flow entered the tee test section and that liquid drops sprayed at the duct inlet reached equilibrium size, distribution and velocity. The side-branch and downstream ducts were 60 and 70 cm long, respectively. The blowers provided an inlet duct cross-section average velocity range of 15–56 m/s. The duct was constructed of Lexan top and bottom walls to permit visual and photographic observation.

Both the downstream and side branches of the tee were equipped with centrifugal cyclone phase separators. The liquid collected in the separators was drained and measured to determine, along with measured air flow rates, the time-averaged flow qualities in the branches. Flow resistances of the side and downstream branches were varied downstream of the separators to control the side/downstream gas flow ratio. Air was saturated at the blower inlet to help prevent drop evaporation.

Dispersed mist phenomena were studied by recording liquid drop and solid particle trajectories photographically. Photography was facilitated by incorporating an antireflection-coated optically flat glass plate as the top wall of the tee test section. The plate was removable for cleaning and for replacement with a Lexan plate containing a grid of tufted needles, which was used for mapping air streamlines. The bottom and side walls of the tee test section contained clear plastic windows to permit illumination, which was primarily by side-scattered light. The source of illumination was electronic flash, either single pulse of variable duration, or a single pulse that was optically chopped (to measure drop velocity) with a stroboscopic frequency of 2880 Hz. The light source was collimated by a slit of adjustable width and oriented in the horizontal plane at mid-duct elevation.

Air streamlines were mapped using the grid of tufted needles. The method is commonly used in aerodynamic testing. The tufts were composed of white threads, approx. 1.5 cm long, with the

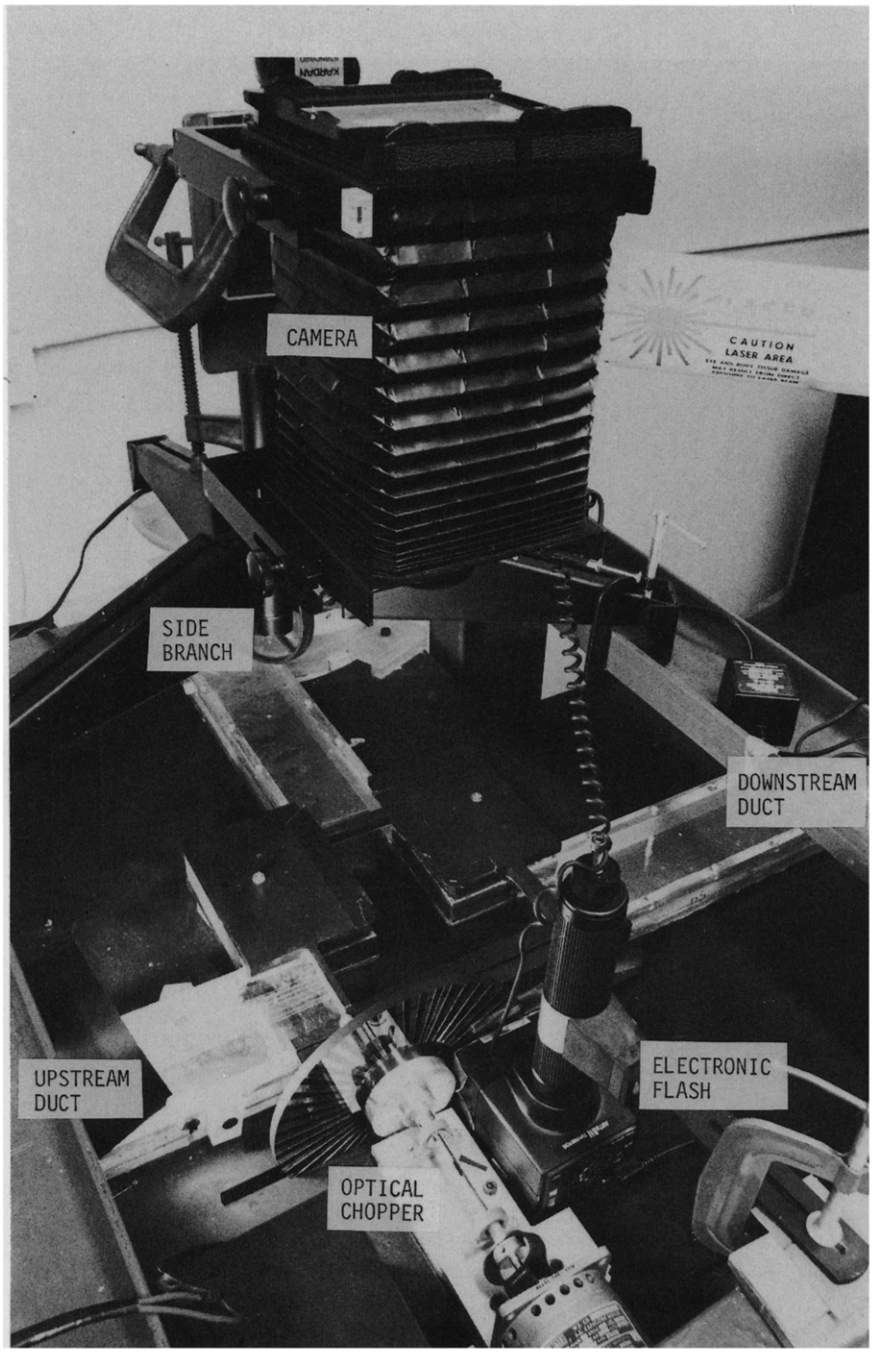

Figure 1. Experimental apparatus: tee test section and instrumentation.

ends of the threads glued to the eyes of needles that projected midway into the flow stream from the top wall. Tufts were also placed next to the wall to map streamlines in the boundary layer. These streamlines diverged from the streamlines in the bulk flow due to a secondary flow component adjacent to the walls.

Water drops were injected at the duct inlet through four hypodermic needles coupled at a continuous flow pump. The needles penetrated the side walls perpendicular to the air flow direction. The air flow broke the liquid jets into drops, which were then entrained. Water drops or solid particles were also injected by means of a hypodermic syringe with the needle penetrating through small holes in the upstream side walls. Solid particles were also injected directly into the eddies to map eddy boundaries.

Table 1. Experiment matrix

Experiment	Upstream velocity: Volumetric flow split, Q_3/Q_1†	Upstream velocity: Midplane average [$\bar{V}_1$(m/s)]	Upstream velocity: Cross-section average [$\bar{V}_1$(m/s)]	Recorded trajectories: Water drops	Recorded trajectories: Latex spheres	Recorded trajectories: H_2O high magnification	Flow map: Liquid mass balance, $\dot{m}_{L3}/\dot{m}_{L1}$	Flow map: Eddies	Flow map: Primary and boundary flows	Flow map: ΔP loss	Flow map: Drop size spectra	Flow map: P_{Eddy} (static)
1	0.428	43.2	38.4	X			0.03 ± 0.01	X	X	X		X
2	0.415	56.0	49.0	X			0.025 ± 0.01		X	X		X
3	1	32.2	28.2	X	X	X		X	X			
4	1	40.0	35.0					X	X			
5	0.59	15.3	13.4					X				
6	1	15.0	13.1					X				
7	0.67	35.8	31.3	X	X	X	0.15 ± 0.03	X	X	X		X
8	0.67	48.7	42.6	X	X	X	0.10 ± 0.03	X	X	X		X
9	0.405	43.3	37.9						X	X		
10	0.41	58.9	51.5								X	
11	0	47.2	41.3								X	
12	0	64.9	56.8									
13	0.25	38.2	33.4	X			0.05 ± 0.03	X	X	X		X
14	0.88	32.6	28.5					X		X		X
15	0.078	35.0	30.7							X		

†3 = Side branch, 1 = upstream.

EXPERIMENT DESCRIPTION AND RESULTS

The following text describes the experiments and presents the results from the larger work (McCreery 1988). Quantitative details of the experiment results are extensively listed in McCreery (1988). Individual experiments were conducted within the framework of a matrix (table 1), which was designed to encompass as wide a range of air volumetric flow ratios Q_3/Q_1 (0.0–1.0) and cross-section average upstream velocities (13–57 m/s) as the experimental apparatus permitted. Quantities measured in the experiments included: gas velocity profiles; pressure measurements; macroscopic mass balances; bulk flow, boundary layer streamline and eddy boundary flow maps; and drop and solid particle trajectories.

PRESSURE AND VELOCITY MEASUREMENTS AND CALCULATED LOSS COEFFICIENTS

Static pressure or pressure changes were measured at typically 10 locations for each experiment (figure 2). The locations were chosen to provide: static pressures and pressure gradients in the upstream, downstream and side branches; static pressure in the corner and downstream eddies; and pressure gradient in the downstream eddy.

The static pressure measurements (table 2) were used along with velocity measurements to calculate loss coefficients across the tee from the upstream to side branch (K_{13}), where K is loss coefficient, and from the upstream to downstream branch (K_{12}) (figure 3). Velocities were measured with static–dynamic pitot tubes. Average velocities were obtained by traversing the duct width by a pitot tube and assuming a 1/7th power velocity distribution in the vertical direction, which is appropriate for the range of Reynolds numbers encountered, approx. Re = 30,000 to 100,000 (Schlichting 1960). This assumption was confirmed by measurements. A typical velocity traverse is shown in figure 4.

Loss coefficients K_{1i}, with $i = 2$ or 3, were defined for a tee by use of Bernoulli's equation, such that

$$P_i - P_1 = \frac{\rho}{2}(V_1^2 - V_i^2) - K_{1i}\frac{\rho}{2}V_i^2 \qquad [1]$$

where P is pressure, V is velocity and ρ is density.

The loss coefficients were used in the phase separation models to calculate flow rates from pressure boundary conditions. The loss coefficients agree well with those of other researchers

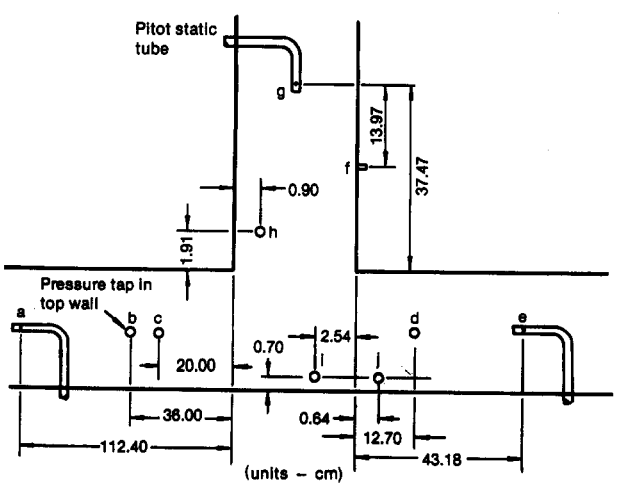

Figure 2. Static pressure measurement locations.

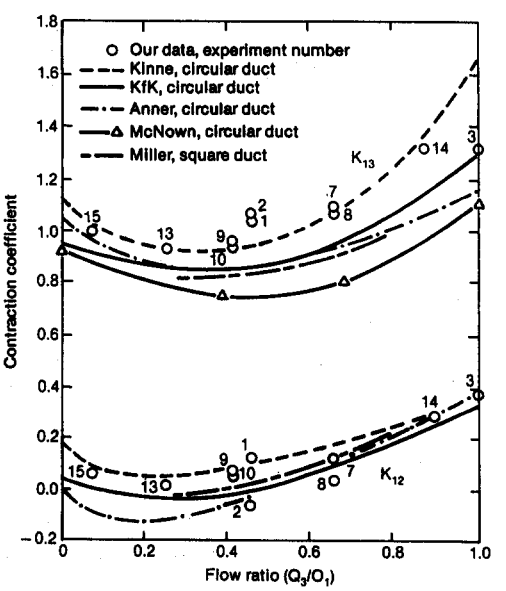

Figure 3. Side-branch and downstream loss coefficients.

Table 2. Static pressure measurements and calculated loss coefficients

Experiment	Pressure units ($Pa \times 10^{-2}$)											
	P_a†	ΔP_{ab}	P_c	P_g	P_e	ΔP_{fg}	ΔP_{de}	P_n	P_i	P_j	K_{13}	K_{12}
1	15.37	4.83	9.57	7.70	16.50	0.02	−0.10	3.00	14.75	14.70	1.02	0.15
2	27.62	9.33	16.42	15.27	29.70	0.04	−0.15	6.16	28.50	28.45	1.09	−0.03
3	24.85	2.32	22.07	15.31	25.23	0.10	+0.02	—	—	—	1.30	0.39
4	—	—	—	—	—	—	—	—	—	—	—	—
5	—	—	—	—	—	—	—	—	—	—	—	—
6	—	—	—	—	—	—	—	—	—	—	—	—
7	20.22	3.35	16.20	12.28	21.74	0.03	+0.20	6.85	20.90	20.95	1.10	−0.02
8	38.45	6.08	31.15	23.60	41.00	0.05	+0.32	13.35	40.35	40.38	1.09	0.05
9	11.96	4.57	6.47	5.18	12.10	0.03	−0.07	1.10	3.88	10.23	0.97	0.07
10	21.96	8.42	11.86	10.10	23.50	0.07	−0.02	2.40	19.18	21.05	0.94	0.06
11	—	—	—	—	—	—	—	—	—	—	—	—
12	—	—	—	—	—	—	—	—	—	—	—	—
13	17.42	3.47	13.25	13.50	16.41	0.02	+0.03	—	—	—	0.95	0.02
14	25.52	2.46	22.57	16.70	25.58	0.02	+0.12	9.37	19.59	19.50	1.34	0.30
15	20.12	2.93	16.60	16.58	16.93	0.03	+0.28	—	—	—	1.00	1.00

†Measurement location defined in figure 2.

Table 3. Macroscopic mass balance

Experiment	Q_{L1} (cm³/min) (±1%)	Q_{G1} (m³/min) (±2%)	$1-X_1$ (±2%)	$\dot{m}_{L3}\dot{m}_{L1}$ (±30%)	$1-X_2$ (±3%)	$1-X_3$ (±30%)	$\frac{1-X_3}{1-X_1}$ (±35%)
1	30.3	4.46	5.6×10^{-3}	0.025	9.4×10^{-3}	3.1×10^{-4}	
1	60.2	4.46	0.011	0.03	0.019	7.8×10^{-4}	0.060
1	60.2	4.46	0.011	0.035	0.022	9.1×10^{-4}	
2	30.3	5.69	4.3×10^{-3}	0.02	7.5×10^{-3}	2.0×10^{-4}	
2	60.2	5.69	8.7×10^{-3}	0.025	0.015	5.0×10^{-4}	0.050
2	60.2	5.69	8.7×10^{-3}	0.025	0.015	5.0×10^{-4}	
7	60.2	3.635	0.014	0.15	0.035	3.0×10^{-3}	0.22
8	60.2	4.95	0.010	0.010	0.072	1.5×10^{-3}	0.15
13	60.2	3.88	0.013	0.015	0.017	7.6×10^{-9}	0.06 ± 50%

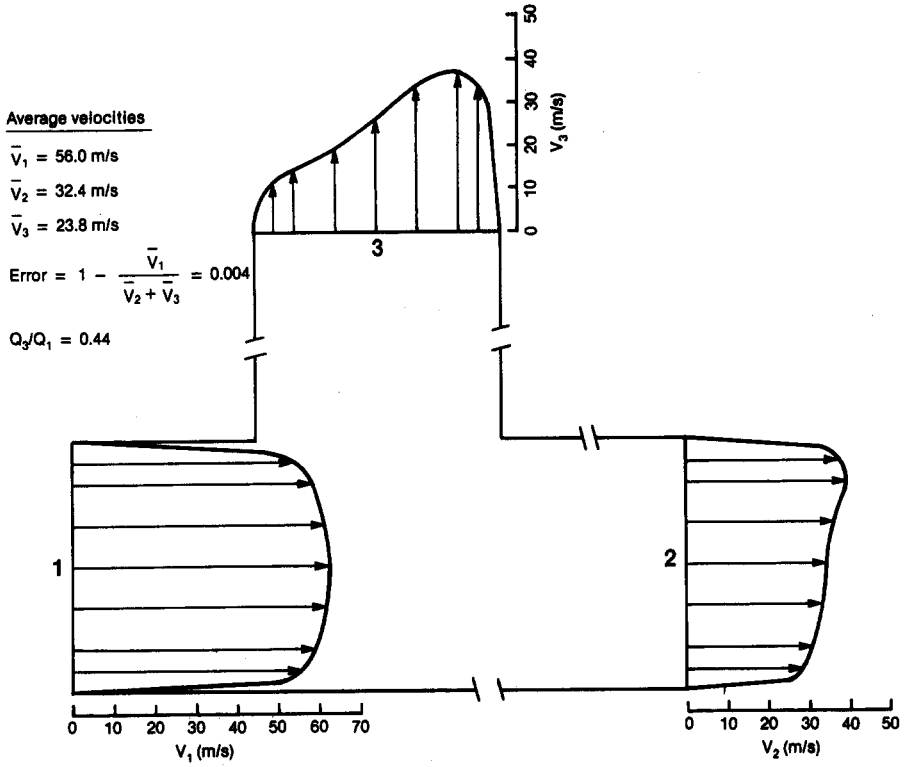

Figure 4. Measured velocity profile for experiment 2.

(Anner 1968; Collier 1976; Reimann *et al.* 1980; Miller 1971; McKnown 1954). All of these data are for circular cross-section tees with the exception of the data of Miller (1971), which is for square cross-section tees.

MACROSCOPIC MASS BALANCES

Macroscopic mass balances were obtained for several of the experiments. From these measurements the liquid separation ratio, defined as $(1 - X_3)/(1 - X_1)$, where X is quality, was calculated (table 3). This ratio, rather than X_3/X_1, was used because qualities are close to 1.0 for our dispersed mist data. The liquid separation ratio was used to test the computer calculations.

The accuracies of the mass balances are sensitive to both liquid storage in the eddies and to drop evaporation. The liquid storage problem was greatly reduced by spraying water into the system for several minutes and then draining the separators before measurements were taken. The evaporation problem was reduced by saturating the inlet air to the blowers. This was accomplished by continuously spraying a filter placed over the blower inlet with water and by performing the experiments on cool, foggy mornings. The accuracy of the mass balances were determined primarily by the collection efficiency of the phase separators, which is 80–90%.

A peculiar and highly nonlinear feature of the flow was observed at high ratios of Q_3/Q_1 ($\gtrsim 55\%$) and was reflected in the mass balances for experiments 7 and 8. Liquid was de-entrained and deposited in the downstream eddy and accumulates. The majority of this liquid was eventually reinjected back into the downstream flow (either as entrained drops or rivulets, depending on the magnitude of velocity V_2). However, a small amount of liquid flowed to the intermittent separation region at the leading edge of the downstream eddy (figure 5). This liquid pool was intermittently swept away as a clearly observable rivulet and followed the air streamline at the wall that originates from this position (the liquid rivulet followed the air streamline because it has low momentum in comparison with the air). This streamline, and therefore the liquid flow, terminated in the corner eddy. Liquid was thereby pumped from the downstream branch into the side branch. All liquid that exited in the corner eddy was observed to eventually be swept out of the side branch, although the flow paths were quite contorted (figure 6). The mass balances for experiments 7 and 8 indicated

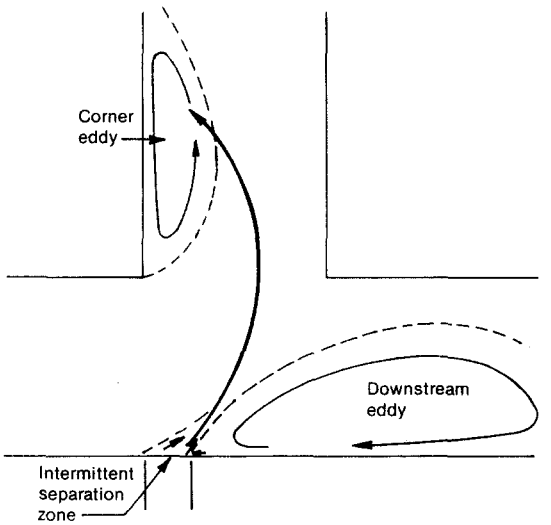

Figure 5. Eddy hopping liquid rivulet, $Q_3/Q_1 = 0.7$.

that this phenomenon was the dominant mechanism for collecting liquid in the side branch for these two cases. The air streamlines at the wall are examined in the latter part of this article and in part II which deals with analysis (McCreery & Banerjee submitted). A model of the quantity of liquid ejected from the downstream eddy that flows to the corner eddy has not yet been developed.

DROP DIAMETER DISTRIBUTION

The process of liquid jet breakup in a spray nozzle produces a large drop size distribution over several orders of magnitude (as does drop production by entrainment, but at typically smaller average size for the same gas velocity). Since drop trajectories in a tee depend to first order on drop diameter, an accurate size distribution is necessary for accurate calculation of phase separation.

The method employed to measure drop diameter was adapted from a method used by Lee & Tankin (1984) and Aihara *et al.* (1985), and is, in their and our experience, simple and reasonably accurate. An oil-coated glass slide is very quickly dipped into the air stream perpendicular to the flow and removed. The drops impacted in the oil film are then measured under a microscope (Unitron measuring microscope). The sample must be sufficiently sparse to avoid drop overlap or coalescence in the film. Drops may also fracture on impact. To avoid these problems, the drops measured were confined to those that were removed from their nearest neighbors by at least several diameters and were spherical in shape. Because of the broad distribution of drop diameters, many size measurements (approx. 350/experiment, for the two experiments performed) were necessary for statistically meaningful results.

The drop size distribution for experiment 11 is shown in figure 7. The distribution for experiment 12 is similarly described by a lognormal distribution function.

The results of the experiments, as reported in McCreery (1988) are that the drop diameter distributions follow a lognormal distribution [as expected from the results of the other researchers, e.g. Podvysotsky & Shraiber (1984)], with the mean drop diameter predicted to within $\pm 6\%$ by the Nukiyama–Tanasawa (1938) correlation, cited in Wallis (1969). The maximum drop diameters observed were predicted by a maximum Weber number, We, the ratio of dynamic pressure force divided by surface tension force ($= \rho_G V^2 d_{max}/\sigma$), equal to 17 ± 2.5. This value is consistent with the values given by Koestel *et al.* (1980) and others. If the drops are formed by entrainment rather than spray, the maximum drop diameter will be similar to that for spray with the same gas velocity. However, the mean drop diameter will typically be smaller and may be calculated from several published correlations, e.g. Lopes & Dukler (1985).

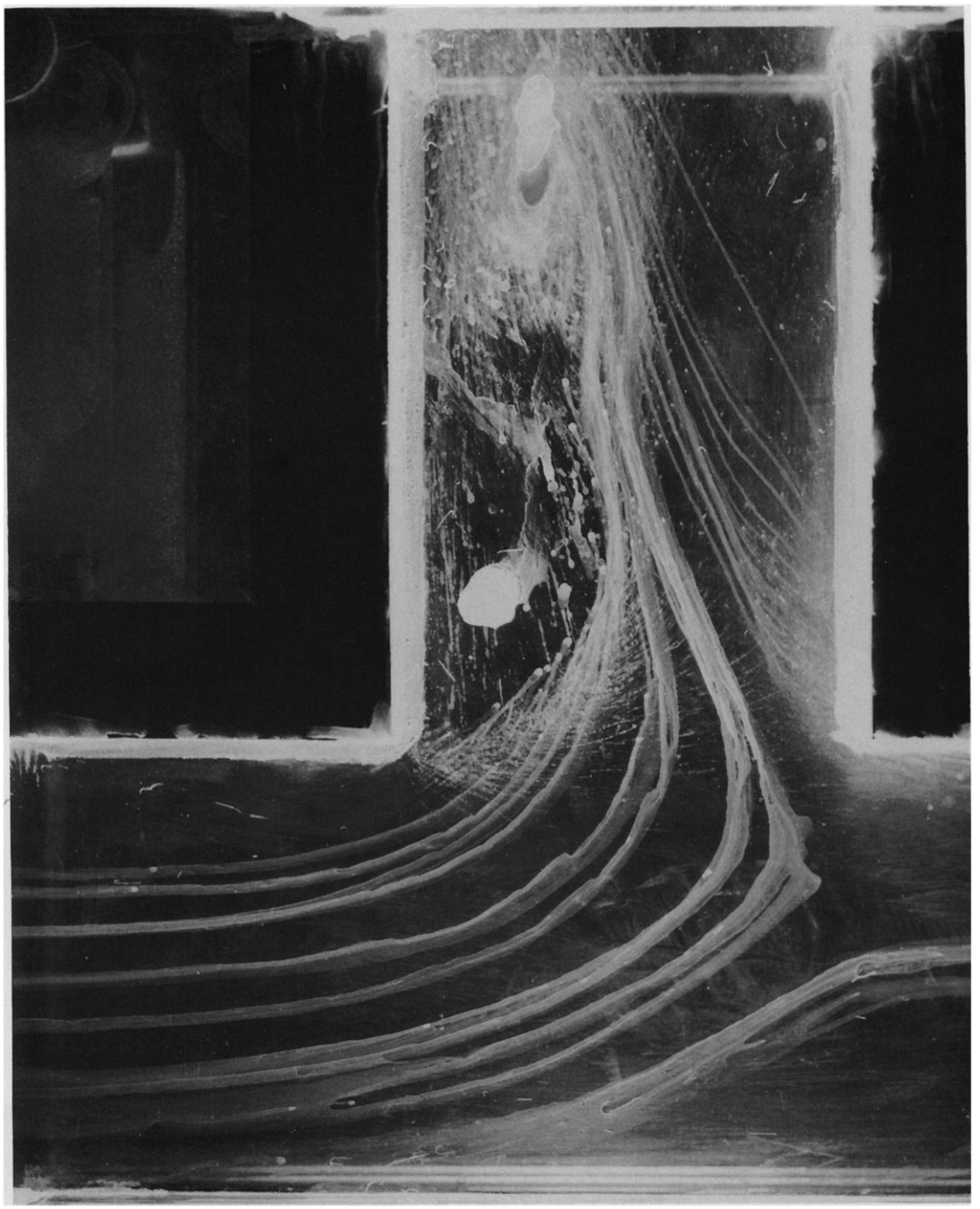

Figure 6. Liquid rivulet pathlines, experiments 1 and 2.

AIR STREAMLINES

Air streamlines outside the corner and downstream eddies were mapped for bulk flow (outside the boundary layers) and at the top and bottom walls. The eddy boundary geometry was mapped and the results compared with models and correlations. The eddy boundary coordinates were used for the computer model input, and the calculated bulk flow streamlines were then tested by comparison with experiments. The bulk air flow was the continuum in which discrete drop trajectories were calculated. These streamlines diverge from the bulk flow streamlines due to a secondary flow component. Air streamlines mapped at the wall provided a comparison for calculated streamlines.

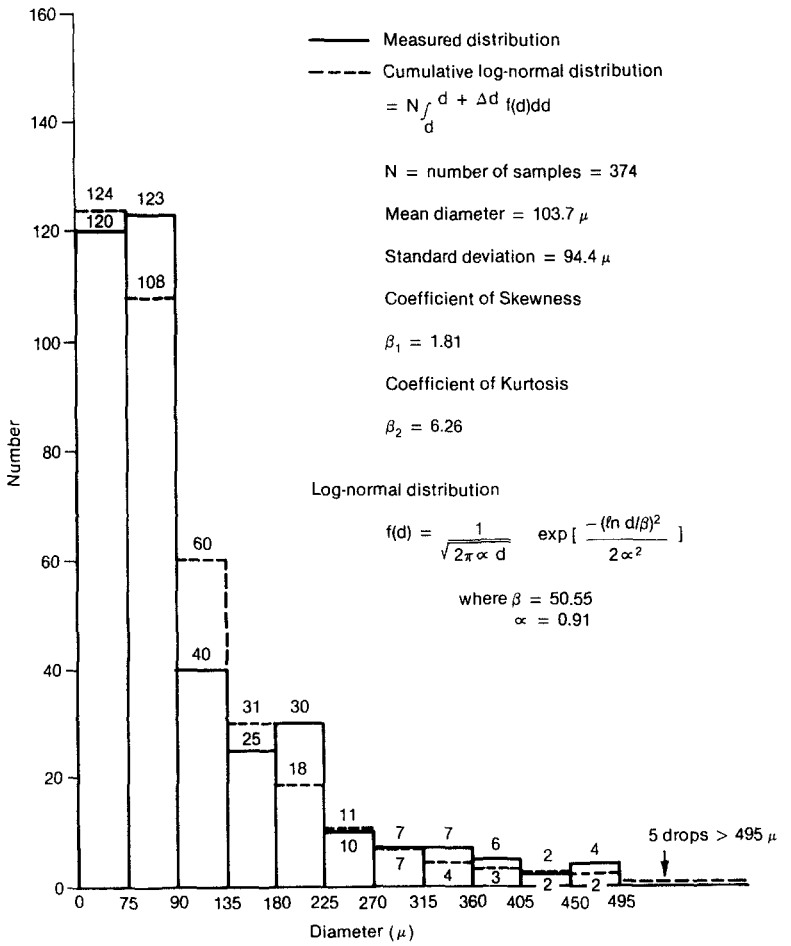

Figure 7. Drop diameter distribution for experiment 11.

Eddy geometry was mapped primarily by solid tracer particles. Additional information was obtained from the grid of tufted needles and from rivulet flow photographs, although the eddy boundaries at the wall were distorted from those of the bulk flow due to secondary flow. The solid tracer particles used were microballoons, which are spherical silica vesicles enclosing nitrogen gas. Photographs of clouds of microballoons trapped in the eddies defined the eddy boundaries.

The contraction coefficient, C, the minimum flow area outside the eddy divided by duct flow area, was measured from the eddy boundary photographs. Conctraction coefficients for the corner and downstream eddies are shown in figures 8 and 9. Contraction coefficients for the corner eddy (C_3) were compared in the figure with the data of Popp & Sallet (1983) and Lemonnier & Hervieu (1988) and with the value determined from free streamline theory, also given by Popp & Sallet (1983). The agreement with both was good.

Contraction coefficients for the downstream eddy (C_2) were the first to be measured over the whole range of flow ratios from 0.0 to 1.0. The contraction coefficients agreed reasonably well with the simplified free streamline theory calculated values, $C_2 = (1 - Q_3/Q_1)$.†

†This equation was derived directly from the Bernoulli equation for flow along the eddy boundary streamline. It was assumed that no pressure loss occurs within the eddy from its upstream position to its vena contracta because of low velocity within the eddy (the usual free streamline theory assumption). As a result of this assumption the velocity along the bounding streamline remains constant. Since, as found in our experiments, the eddy starts a short distance upstream of the side branch and within the upstream duct (figure 6), then V_2 at the contraction approximately equals V_1 (assuming a uniform velocity distribution across the flow at these two locations, which from our experiments is seen to be a reasonable but not exact assumption) and application of continuity yielded this equation.

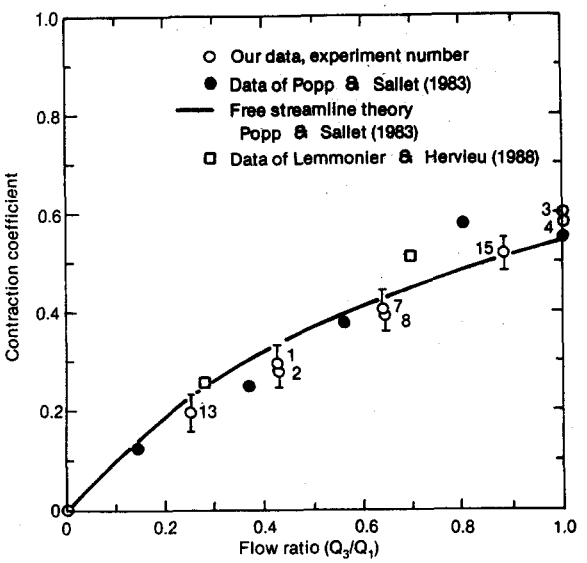

Figure 8. Experimental and theoretical values of the corner eddy contraction coefficient.

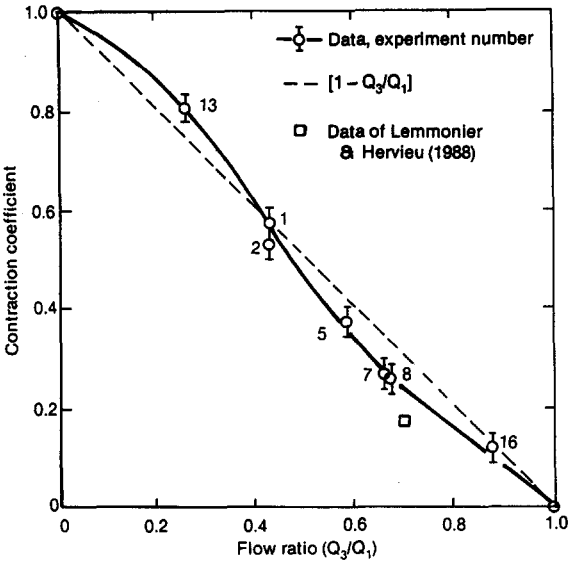

Figure 9. Downstream eddy contraction coefficient.

One downstream contraction coefficient may be calculated from the data presented by Lemonnier & Hervieu (1988). It agrees reasonably well with our data.

Bulk flow was mapped outside the eddy boundaries by use of photographs of the grid of tufted needles. Information obtained from the photographs was combined with eddy boundary geometry and potential flow theory to graphically obtain the maps. The method assumes that the turbulent flow outside the eddies and boundary layers conforms to potential flow, the commonly employed "infinite Re assumption". The air streamlines for two representative experiments (experiments 1 and 2) are shown in figure 10. The streamlines were seen in the experiments to depend upon the flow ratio Q_3/Q_1, but not velocity. This is expected if the infinite Re assumption is valid and the flow conforms to potential flow.

Streamlines at the wall were mapped by use of the grid of tufted needles with tufts adjacent to the top wall and by injection of water rivulets attached to the bottom wall. The rivulets contained a suspension of titanium dioxide for increased contrast. The rivulets were seen to follow the wall streamlines closely (figure 11); the rivulets aligned with average tuft direction. The instantaneous positions shown in the figure may deviate from the average by up to 10° or 15° due to turbulent fluctuations. The rivulets aligned with the streamlines because the liquid had low momentum compared with the air (a ratio of <0.1, from measured rivulet velocity), and are dragged by the air. The photograph is a multiple exposure, which also illustrates microbaloons injected into the downstream eddy.

Rivulet pathlines are shown in figures 12 and 6 for $Q_3/Q_1 = 0.67$ (experiments 6 and 7) and $Q_3/Q_1 = 0.41$ (experiments 1 and 2), respectively. The rivulets in the first figure diverged and flowed into either the downstream duct or into the side branch. The rivulets in the second figure flowed exclusively into the side branch. This is consistent with the observed "eddy hopping" rivulets observed for dispersed mist flow, since the upstream position of the downstream eddy for experiments 6 and 7 is close to where the outermost rivulet in figure 12 breaks away from the wall (the rivulet is injected by hypodermic needle directly onto the wall opposite the side branch). An eddy hopping rivulet would, therefore, follow a path close to this.

In addition to rivulets, a thin (but not even or continuous) film was created by mixing a wetting agent (Kodak Photoflo solution) with the injected water. The film was observed to follow essentially the same path as rivulets.

A feature of rivulet or thin film flow is that the liquid never exactly follows the streamline at the wall that impacts the downstream side branch corner and divides the flow. The vorticity of the gas, and therefore of the liquid, increases with the decrease of the radius of curvature for streamlines approaching the corner, and the liquid is therefore deflected to one side or the other

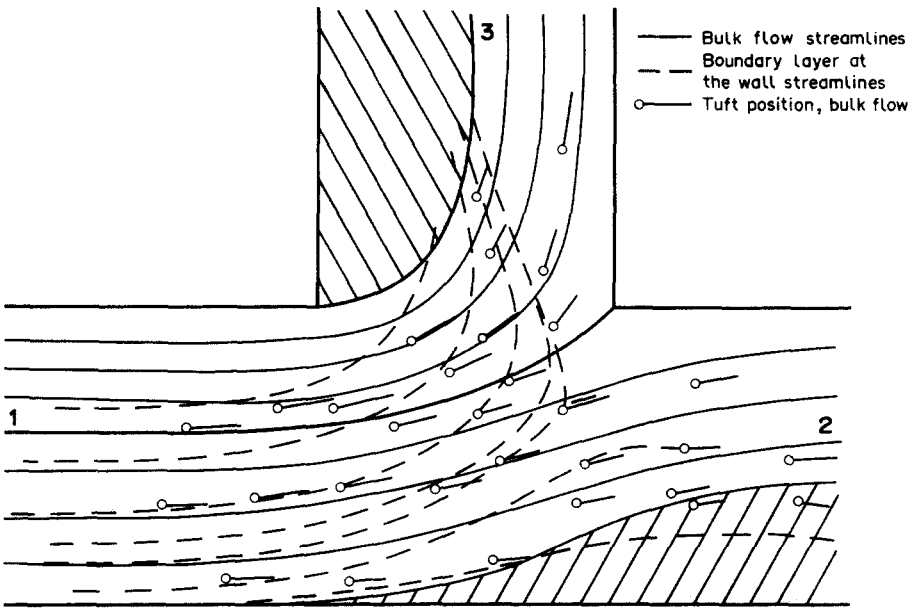

Figure 10. Air streamlines, experiments 1 and 2.

before impacting the corner (this deflection is predicted by the models discussed in part II (McCreery & Banerjee submitted).

WATER DROP AND SOLID PARTICLE TRAJECTORIES

Drop and solid particle trajectories were mapped and used in conjunction with air streamlines and velocities to determine drop drag coefficients. This was accomplished by employing the drop trajectory code and testing various drop drag coefficient vs drop Re correlations until agreement was obtained over a range of Re. In order to accomplish this task, drop or solid particle diameter and velocity as a function of pathlength were needed for each recorded trajectory to be compared with calculations. The trajectories were recorded photographically in side-scattered illumination with, in some experiments, the electronic flash pulse optically chopped to measure drop or solid particle velocity.

Stroboscopic photographs of drop trajectories were made to investigate the relationship of drop and gas velocity at the tee inlet. A comparison of the measured drop velocity with the average gas velocity showed that the two are approximately equal for the range of gas velocities and drop diameters investigated (approx. 20–300 μm). The drop velocity had a fairly flat distribution across the duct. The fact that the velocity distribution was fairly uniform agrees with the results of Lourenco *et al.* (1983).

Drop diameters for large diameter drops ($> 100\ \mu$m) were measured from the width of recorded streak lines in enlargements of full field photographs. The photographs were made on 10.1×12.7 cm sheet film with a magnification of approx. 1 : 1 (image/object dimension). The streak line image contrast was increased greatly by the addition of submicron size titanium dioxide particles in dilute suspension to the water injected. Smaller drops required larger magnification photographs (approx. 3 : 1 on the image plane and approx. 25 : 1 on enlargement) with a smaller field of view than the complete tee (figure 13). The slope of the trajectories in the center of the high magnification photographs was then related to drop diameter. The slope of drop trajectories that passed through the central position of the small field of view in the full field photographs determined the drop diameter of these smaller drops. The accuracy of determining drop diameter by this method is approx. 10–20 μm and is determined primarily by film resolution.

In addition to water drops, the trajectories of solid particles of known size and density were recorded. The solid particles were commercially available Lexan spheres (Bangs 1984). The particles which proved to be the most useful for trajectory mapping had a diameter of $45 \pm 7\ \mu$m, and a specific gravity of 1.05. As expected, the trajectories of the solid particles were close to those of

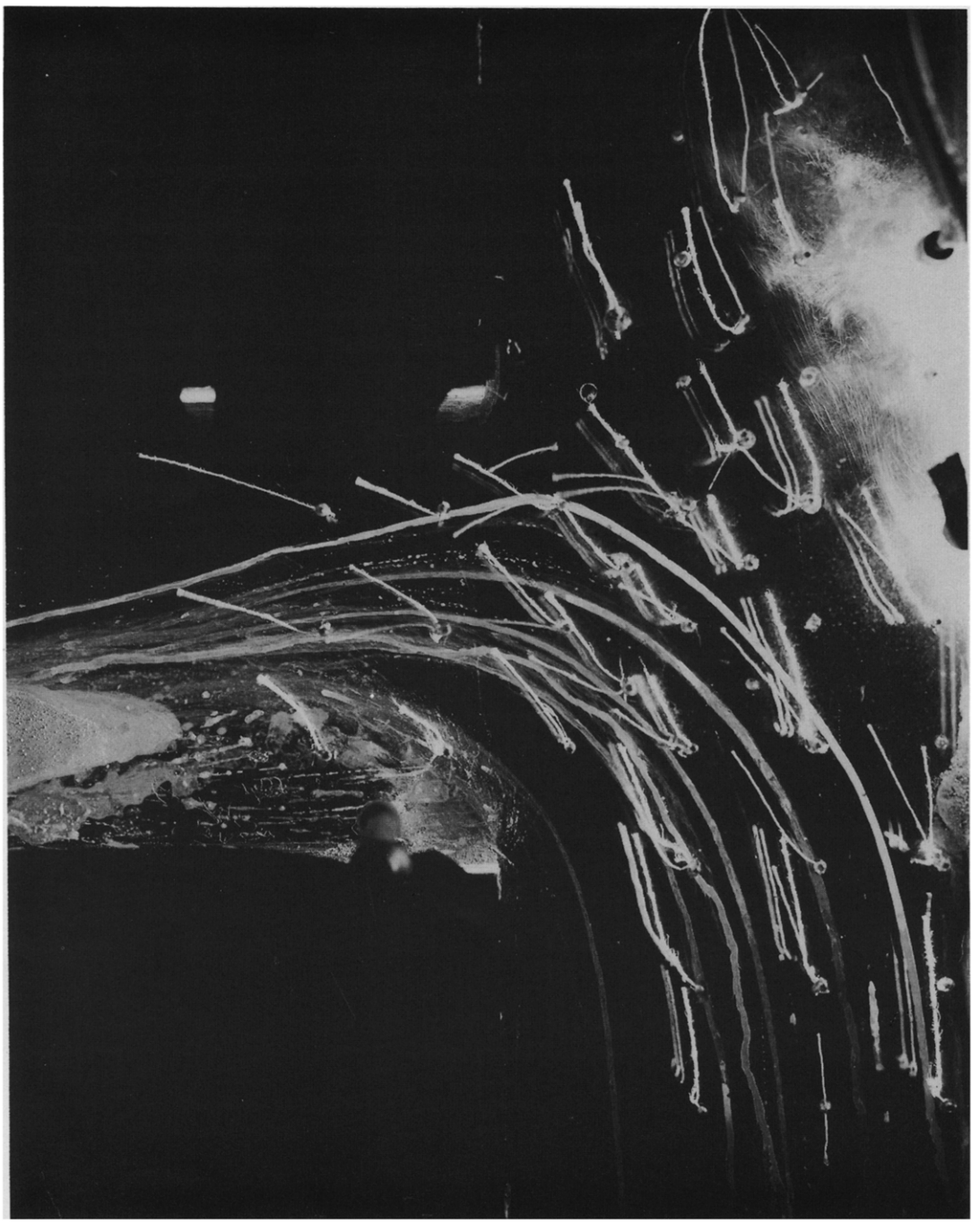

Figure 11. Tufted needle position for bulk flow, rivulets, experiments 1 and 2.

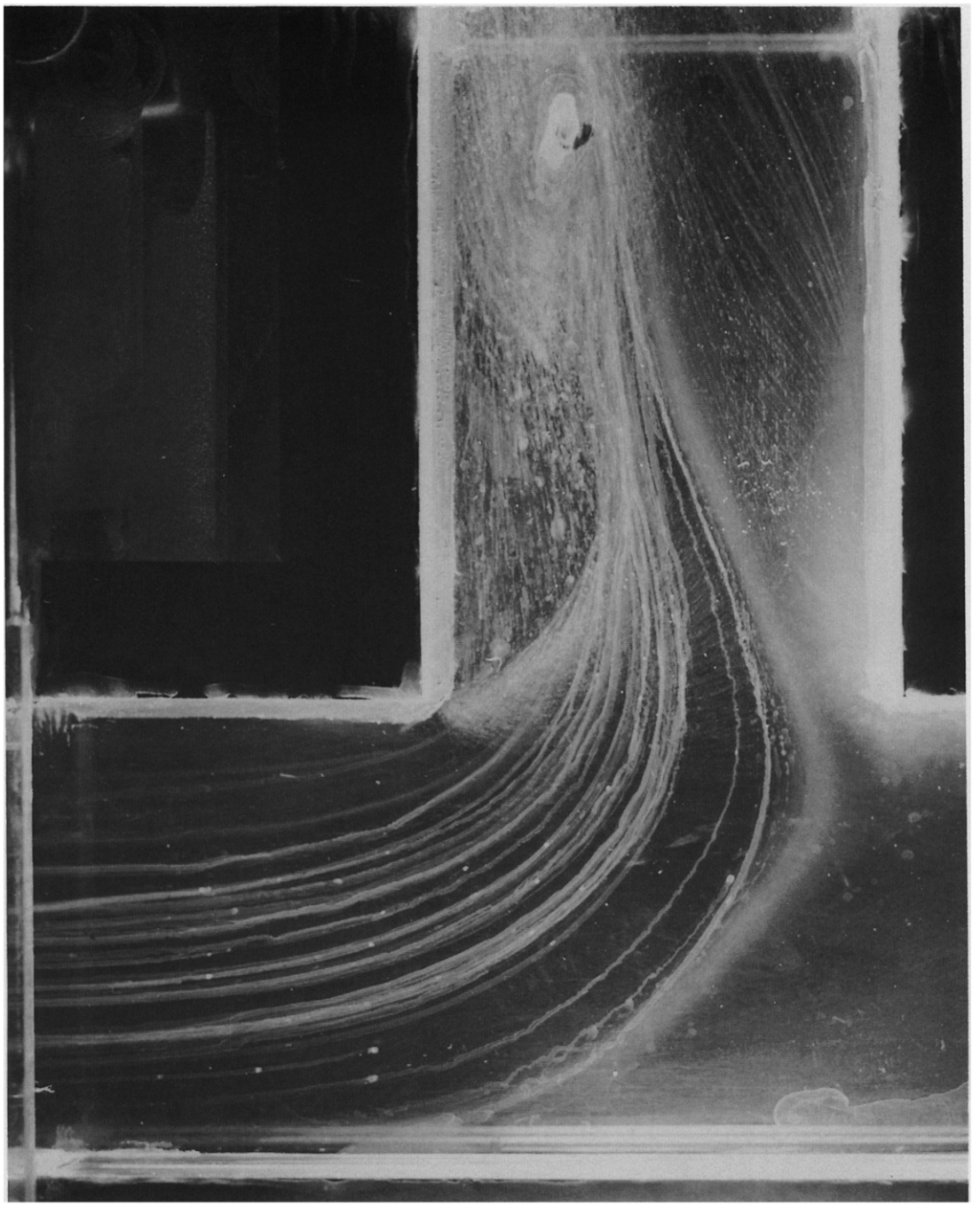

Figure 12. Rivulet pathlines, experiments 7 and 8.

water drops of the same diameter because the drag coefficient of small drops [$\lesssim 400\ \mu$m according to Clift *et al.* (1978)] was approximately the same as that of solid particles of the same diameter. This is because of increased surface tension force that held the drops spherical and the decreased internal circulation within small drops.

A significant feature of the trajectories is the smoothness of the curves they describe. The trajectories appear relatively unaffected by velocity fluctuations of the higher turbulent flow. The reason is that the diffusivity of the particles, which are much larger than the finest eddy structures ($\leqslant 0.5\ \mu$m) and of higher density than the air, is at least an order of magnitude less than the turbulent air diffusivity (Trela *et al.* 1982). Because of their insensitivity to turbulent fluctuations, drop trajectories, for the drop size ranges of interest for dispersed mist flow,

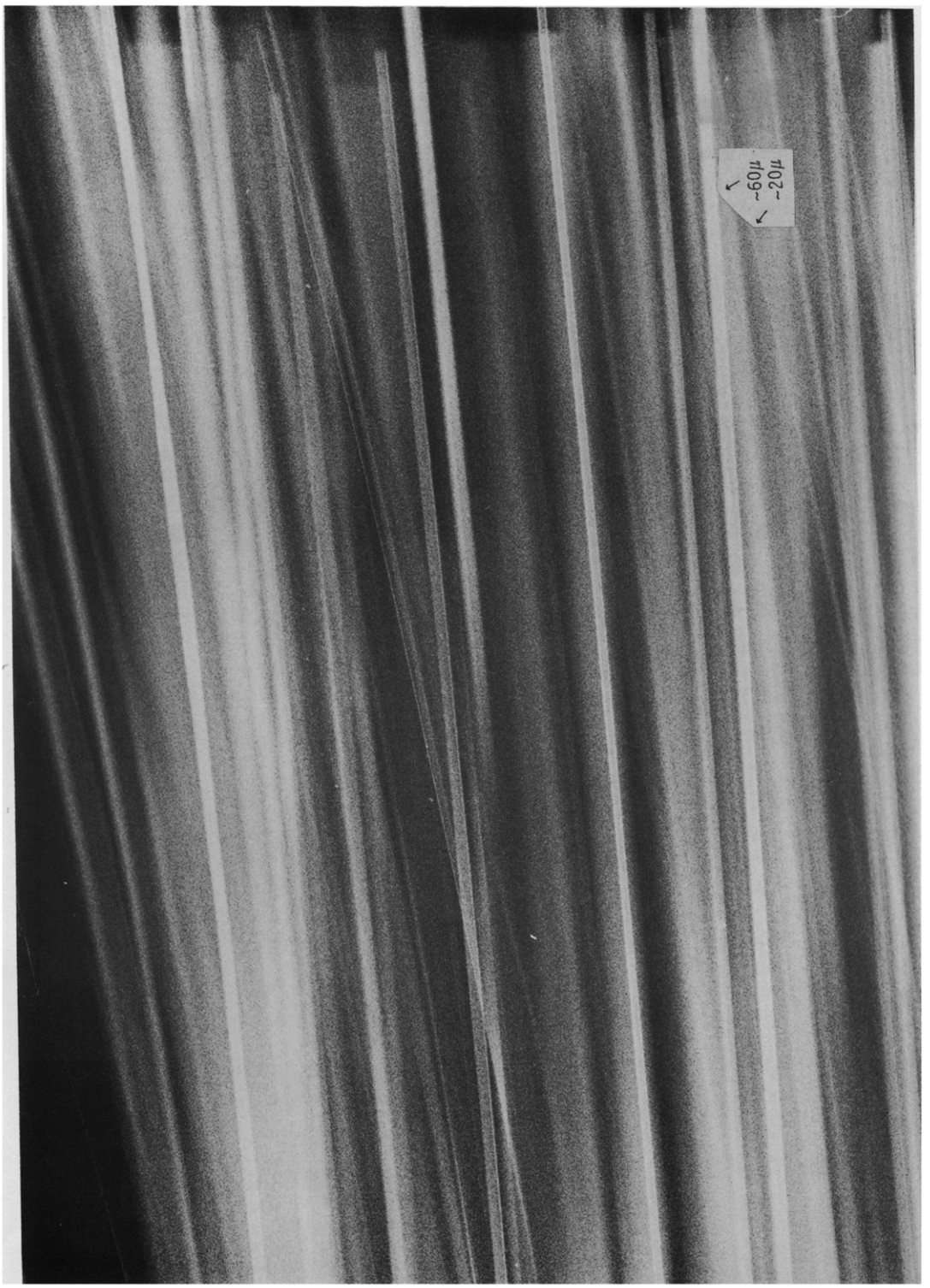

Figure 13. Magnified drop trajectories.

may be modeled accurately by considering only the mean air velocity distribution. For very high velocity flow ($\lesssim 200$ m/s) this conclusion might no longer be valid due to the small size of entrained drops.

CONCLUSIONS

An experimental investigation of dispersed mist and dispersed annular (rivulet or thin film) flow phase separation in a tee was performed. The experiments were used to help formulate and test mechanistic analytical models of phase separation in a tee for these flow regimes. Measurements included gas velocity profiles, pressure measurements, macroscopic mass balances, photographically recorded streamline and eddy boundary flow maps, and drop and solid particle trajectories.

The velocity and pressure measurements were combined to calculate loss coefficients. The values of the loss coefficients agree well with the values of the loss coefficients for circular and square cross-section tees.

Macroscopic mass balances were obtained for dispersed mist flow for several experiments. The measurements were sensitive to evaporation and liquid storage in the eddies, but they provided acceptable accuracy for model testing.

A highly nonlinear phenomena which significantly affects mass balances was observed in experiments with flow ratios $Q_3/Q_1 \gtrsim 0.55$. Drops were de-entrained and collected in the downstream eddy. A significant fraction of this liquid broke away from the front of the downstream eddy and was swept along the bottom wall by the air into the corner eddy. The occurrence of this newly observed phenomena is the dominant mechanism for providing liquid flow out the side branch of the tee in the high flow ratio experiments.

Drop size distribution for dispersed mist flow was measured and compared with the results of several other researchers. The diameter distribution is best described by a lognormal distribution.

Air streamlines and eddy boundaries were mapped for both the bulk flow and for the top and bottom wall flow. Air streamlines at the wall diverged from those of the bulk flow due to a secondary flow component within the boundary layer. It was observed that liquid rivulets or thin films follow the air streamlines at the wall.

Corner and downstream eddy contraction coefficients were obtained from the eddy boundary maps. Corner eddy contraction coefficients compare well with those obtained by other researchers and from free streamline theory. Contraction coefficients for the downstream eddy were the first obtained over the whole range of flow ratios from 0.0 to 1.0 and agree reasonably well with a simple free streamline theory.

Drop and solid particle trajectories were mapped photographically for a variety of sizes. The trajectories describe smooth curves that are insensitive to local turbulent velocity fluctuations.

Acknowledgements—We wish to thank Ontario Hydro, and specifically W. I. Midvidy, for providing financial and technical support for this research. We also thank Professors H. Fenech and T. G. Theofanous for helpful and stimulating discussions.

The work at Idaho National Engineering Laboratory was performed, in part, under the auspices of the U.S. Department of Energy, DOE Contract No. DE-AC07-76ID01570.

REFERENCES

AIHARA, T., SHIMOYAMA, T., HONGOH, M. & FUJINAWA, K. 1985 Instrumentation and error sources for the measurement of the local drop-size distribution by an immersion-sampling cell. In *Proc. 3rd Int. Conf. on Liquid Atomisation and Spray Systems*, Institute of Energy, Paper VC-5.

ANNER, L. 1968 *Investigation of Flow Losses in Mine Ventilation*. Freiberger Forschunghefte, VEB, Leipzig.

BANGS, L. 1984 *Uniform Latex Particles*. Seragen, Indianapolis, Ind.

CLIFT, R., GRACE, J. R. & WEBER, M. E. 1978 *Bubbles, Drops, and Particles*. Academic Press, New York.

COLLIER, J. G. 1976 Single-phase and two-phase flow behavior in primary circuit components. In *Proc. NATO Advanced Institute on Two-phase Flow and Heat Transfer*, Vol. 1, pp. 313–365. Hemisphere, Washington, D.C.

KOESTEL, A., GIDO, R. G. & LAMKIN, D. E. 1980 Drop size estimates for a loss-of-coolant-accident. Reports NUREG/CR-1067 & LA-8449-MS.

LEE, S. Y. & TANKIN, R. S. 1984 Study of liquid spray (water) in a non-condensable environment (air). *Int. J. Heat Mass Tranfer* **27**, 351–361.

LEMONNIER, H. & HERVIEU, E. 1988 Theoretical modelling and experimental investigation of single-phase and two-phase flow division at a tee-junction. In *ANS Proc. 1988 natn Heat Transfer Conf.*, Houston, Tex.

LOPES, J. C. B. & DUKLER, A. E. 1985 Droplet sizes, dynamics and deposition in vertical annular flow. Report NUREG/CR-4424.

LOURENCO, L., RIETHMULLER, M. L. & ESSERS, J. A. 1983 The kinetic model for gas–particle flows and its numerical implementation. Presented at the *Int. Conf. on the Physical Modeling of Multiphase Flow*, Coventry, U.K.

MCCREERY, G. E. 1988 Investigation of dispersed and dispersed–annular (thin film or rivulet) flow phase separation in tees. Ph.D. Dissertation, Dept of Chemical & Nuclear Engineering, Univ. of California, Santa Barbara.

MCCREERY, G. E. & BANERJEE, S. Phase separation of dispersed mist and dispersed annular (rivulet or thin film) flow in a tee—II. Analysis. *Int. J. Multiphase Flow*. Submitted.

MCKNOWN, J. S. 1954 Mechanics of manifold flow. *Trans ASCE* **119**(2714), 1103–1142.

MIDVIDY, W. I. 1983 Dispersed flow in tee junctions. Ontario Hydro 9199G.

MILLER, D. S. 1971 *Internal Flow. A Guide to Losses in Pipe and Duct Systems*. British Hydromechanics Research Assoc., U.K.

PODVYSOTSKY, A. & SHRAIBER, A. 1984 Coalescence and break-up of drops in two-phase flows. *Int. J. Multiphase Flow* **10**, 195–209.

POPP, M. & SALLET, D. W. 1983 Experimental investigation of one- and two-phase flow through a tee junction. Presented at the *Int. Conf. on the Physical Modeling of Multiphase Flow*, Coventry, U.K.

REIMANN, J., SEEGER, W. & JOHN, H. 1980 Erste experimente zur unverteilung einer luft-wasser-stromung in einem t-stuck. Report KfK 06-01-03P08A.

SCHLICHTING, H. 1960 *Boundary Layer Theory*. McGraw-Hill, New York.

SEEGER, W., REIMANN, J. & MULLER, V. 1985 Phase separation in a T-junction with horizontal inlet, part I: phase separation. Presented at the *2nd Int. Conf. on Multiphase Flow*, London.

TRELA, M., ZEMBIK, J. & DURKIEWICZ, B. 1982 Droplet deposition on a flat plate from an air/water turbulent mist flow. *Int. J. Multiphase Flow* **8**, 227–238.

WALLIS, G. B. 1969 *One-dimensional Two-phase Flow*. McGraw-Hill, New York.